Struct Chem (2009) 20:1055–1065
DOI 10.1007/s11224-009-9509-x

ORIGINAL RESEARCH

Structural and aromatic aspects for tautomerism of (*Z*)-6-((4-bromophenylamino)methylene)-2,3-dihydroxycyclohexa-2,4-dienone

Hasan Karabıyık · Hande Petek · Nazan Ocak İskeleli · Çiğdem Albayrak

Received: 14 May 2009 / Accepted: 28 August 2009 / Published online: 16 September 2009

Abstract The molecular and crystal structure of (*Z*)-6-((4-bromophenylamino)methylene)-2,3-dihydroxycyclohexa-2,4-dienone were determined by single crystal X-ray diffraction and spectroscopic methods. Molecules of the compound can be regarded as a resonance hybrid of *cis*-keto tautomer and zwitterionic form. Pairs of molecules of the compound generate pseudocyclic centrosymmetric $R_2^2(10)$ supramolecular synthons with the aid of O–H···O type intermolecular H-bonds. Stacking of $R_2^2(10)$ synthons along *b*-axis is stabilized by $\pi\cdots\pi$ interactions. Changes in both covalent topology and molecular geometry of the compound accompanying proton transfer were monitored by a relaxed PES scan with respect to hydroxyl bond length used as redundant internal coordinate. Quantum chemical studies at 6-311 + G(d,p) level reveal that bond lengths which are indicative to tautomerization process cannot reach their expected values even if proton transfer occurs in gas phase and pseudo-aromatic chelate ring formation has primary effect on the stabilization of NH tautomer. Resonance-assisted intramolecular H-bond affects the electronic state of its neighboring aromatic fragments.

Keywords Schiff base · Tautomerism · Resonance-assisted H-bond (RAHB) · π-electron coupling · HOMA

H. Karabıyık (✉)
Department of Physics, Dokuz Eylül University, 35160 Buca, İzmir, Turkey
e-mail: hasan.karabiyik@deu.edu.tr

H. Petek
Department of Physics, Ondokuz Mayıs University, 55139 Samsun, Turkey

N. O. İskeleli
Department of Science Education, Ondokuz Mayıs University, 55200 Samsun, Turkey

Ç. Albayrak
Department of Science Education, Sinop University, 57000 Sinop, Turkey

Introduction

The structures of *o*-hydroxy aromatic Schiff bases have received much attention due to their keto–enol (or NH–OH) tautomerism in recent years [1–4]. Depending on the type of tautomer, two types of intramolecular hydrogen bond involving a photochemically or thermochemically induced proton are possible, namely O···H–N in keto (NH) and O–H···N in enol (OH) tautomers. Although the proton-transfer reaction is seemingly straightforward, it causes a change in the π-electronic system and induces large-scale in-plane and out-of-plane skeletal deformations. It is prevalently accepted that OH form is more stable than NH form [5]. In the solid state, while OH tautomeric forms are predominant in salicylideneanilines (SAs) [6], NH forms are also observed crystallographically. OH and NH forms of Schiff bases may coexist in different sites of the same crystal structure [7] or in the same molecular structure [8].

Although Schiff bases exhibit two well-known tautomeric forms, OH and NH, another structural form referred to as the zwitterion is also possible. Zwitterionic form of them is regarded as a variant of their NH forms, but they can be easily distinguished from canonic *cis*-keto tautomers through their N^+–H bond distances. Zwitterionic forms of Schiff bases have a resonance-assisted ionic intramolecular hydrogen bond (N^+–H···O^-) [9, 10], and their N^+–H bonds are considerably longer than the standard interatomic

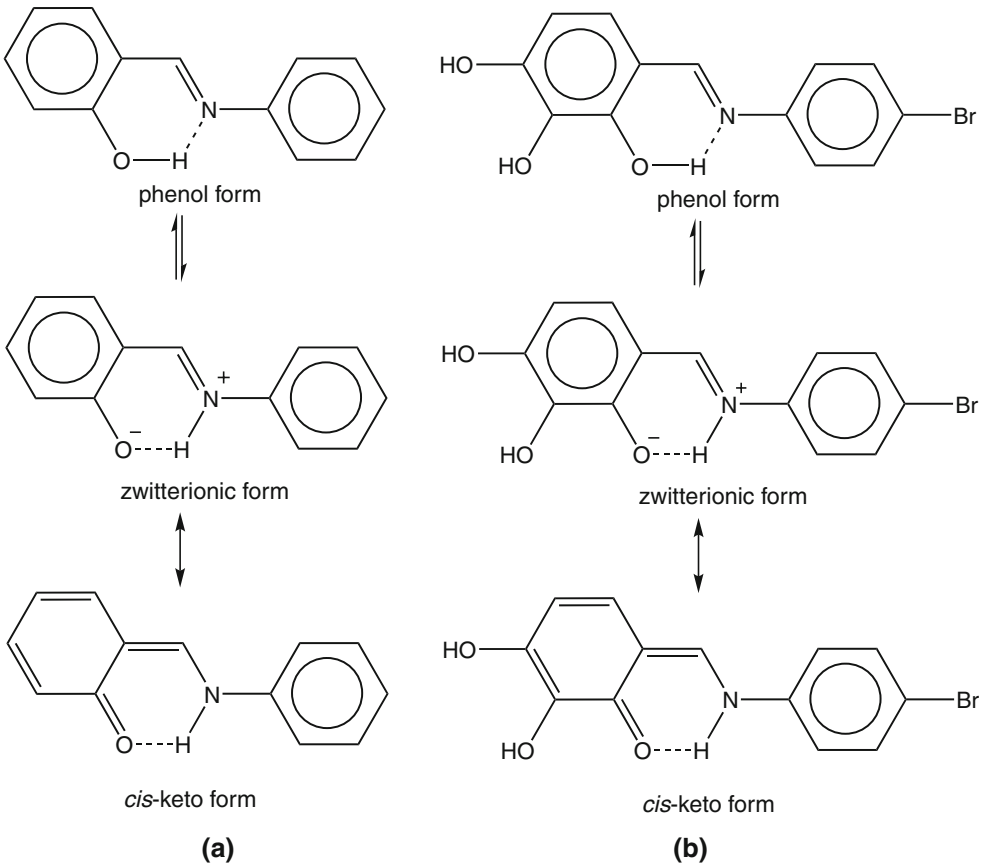

Chart 1 Possible tautomeric forms of SA (**a**) and the title compound (**b**). The *cis* labeling is based on relative positions of tautomeric H and O in *ortho* position

separations observed in neutral N–H bonds [11]. The other ionic bonds in the zwitterions, C=N^+ and C–O^-, are not as distinctive as indicators as is the N^+–H bond, because their molecular structures in the solid state can be regarded as a resonance hybrid of two canonical structures, *cis*-keto tautomer and zwitterionic form [5, 12] (Chart 1a). The predominance of the zwitterionic over NH canonic form of Schiff bases can be discerned from details of their molecular geometries [13]. In this regard, scrutiny of crystal structure combined with quantum chemical studies supplies an efficient probe to be used in their structural classification.

OH forms of *o*-hydroxy aromatic Schiff base derivatives have the expected bond distances in solid state, whereas this is invalid for their NH forms. Structural classification of their NH forms is intricate in solid state due to their intermediate bond distances [13]. As to this aspect, Ogawa and Harada [5, 14] have proposed that NH form of SA derivatives is predominantly zwitterionic in crystals, while it is predominantly quinoidal (canonical NH) in gas-phase or solution and their stabilization is achieved by intermolecular H-bonds in molecular aggregate at low temperature. The bond distances reported by them [5, 14] for a similar SA derivatives do not correspond to those of canonical *cis*-keto form even at 15 K in solid state. This guiding rule requires a detailed discussion in structural sense, since it may lead to structural confusion in the related literature.

We have recently reported an intermediate structure [13] between canonical OH and NH form of a Schiff base compound, having very similar molecular skeleton to that in this study. We show that structural characterization of SA derivatives having regard to only the positions of their tautomeric proton may lead to overlook certain details related to molecular structures of them. In a continuation of our structural interest regarding *o*-hydroxy aromatic Schiff bases, here we report that crystal and molecular structure of (*Z*)-6-((4-bromophenylamino)methylene)-2,3-dihydroxy-cyclohexa-2,4-dienone. Tautomerism process of the compound and its effects on the molecular geometry were examined with the aid of redundant internal coordinate *d*(O–H) as an intramolecular degree of freedom. Such an investigation gives us valuable structural insights about chemical background underlying tautomerism of *o*-hydroxy aromatic Schiff bases.

Experimental

Synthesis and spectral characterization of the compound

(*Z*)-6-((4-bromophenylamino) methylene)-2,3-dihydroxy-cyclohexa-2,4-dienone Was prepared by reflux a mixture of

a solution containing 2,3,4-trihydroxybenzaldehyde (0.1 g 0.65 mmol) in ethanol (20 mL) and a solution containing 4-bromoaniline (0.11 g 0.65 mmol) in 20 mL ethanol. The reaction mixture was stirred for 1 h under reflux. The resulting yellow precipitate was filtered off and crystals of (*Z*)-6-((4-bromophenylamino)methylene)-2,3-dihydroxy-cyclohexa-2,4-dienone suitable for X-ray analysis were obtained from ethanol by slow evaporation (yield 92%; m.p. 477–479 K). Elemental analysis calculated for $C_{13}H_{10}BrNO_3$; C: 50.67, H: 3.27, O: 15.57, N: 4.55%, found C: 50.12, H: 3.54, O: 15.28, and N: 4.15%.

Proton NMR spectra (400 MHz) were recorded with a Bruker DPX FT-NMR spectrometer (TMS as internal standard) at 297 K. ^{1}H-NMR (δ in ppm, $CDCl_3$): 15.38 [d, 1H, N*H*, $^3J_{\underline{N}H-CH} = 7.5$ Hz]; 11.56 [s, 2H, Ar–O*H*]; 9.30 [d, 1H, C*H*, $^3J_{NH-C\underline{H}} = 7.5$ Hz]; 6.84–8.26 [m, 6H, Ar–*H*]. The FT-IR spectrum of the compound was recorded from KBr pellets with an IASCO FT–IR 430 spectrophotometer. IR spectroscopic data (ν, cm^{-1}): 3425 (*br*, C=O···H–N), 3130 (*br*, O–H), 3064 (aromatic CH), 1624 (C=O), 1476–1610 (aromatic C=C), 1328 (C_{Ar}–OH), 1196 (C–N), 495 (C_{Ar}–Br).

X-ray crystallography

A suitable sample of size 0.540 × 0.247 × 0.080 mm^3 was chosen for the crystallographic study and then carefully mounted on goniometer of a STOE IPDS II diffractometer. All diffraction measurements were performed at room temperature (296 K) using graphite monochromated Mo K_α radiation ($\lambda = 0.71073$ Å). The systematic absences and intensity symmetries indicated the monoclinic *P-1* space group. A total of 8631 reflections (1614 unique) within the θ range of [3.10° < θ < 28.09°] was collected in the rotation mode. The crystal sample selected for data collection is non-merohedrally twinned (twin lattice quasi-crystal, TLQS) by a twofold rotation axis perpendicular to (001) with two reciprocal lattices differently oriented, giving rise to double diffraction spot sets with a twinning ratio of 0.51:0.49. We were aware of the twin character of the crystal samples at the data collection stage, but pure crystals giving rise to single diffraction spot set could not be found. Since the partially overlapped reflections arising from non-merohedral character of the crystal sample would not be integrated separately, 684 partially overlapped independent reflections could not be satisfactorily measured and they were discarded from the dataset. As a result of this, the completeness of dataset is reduced to 70%. Although the reaction mixture was recrystallized, the results obtained from new crystal samples in comparison with those presented here have not been further improved. Single-crystal sample of the compound selected for collecting intensity data was in poor quality leading to relatively high R_{int} value of 0.12.

The intensities collected were corrected for Lorentz and polarization factors, absorption correction by integration method via X-RED software [15] and cell parameters were determined by using X-AREA software [15] with the aid of 14,882 reflections in the range of [2.96° < θ < 28.20°]. The structure was solved by direct methods using WinGX's [16] implementation of SHELXS-97 [17]. The refinement was carried out by full-matrix least-squares method on the positional and anisotropic temperature parameters of the non-hydrogen atoms, or equivalently corresponding to 175 crystallographic parameters. All non-hydrogen atoms were refined anisotropically. Aromatic H atoms and H atom hydroxyl group in *para* position were refined using pertinent riding models with C–H distances of 0.93 Å and O–H distances of 0.82 Å. The displacement parameters of H atoms were fixed at 1.2 U_{eq} of their parent carbon atoms for aromatic C–H and 1.5 U_{eq} of their parent oxygen atoms for hydroxyl groups. Remaining H atoms were located difference Fourier map and refined freely. The scattering factors were taken from SHELXL-97 [17]. Other details of the data collection conditions and details of refinement process are summarized in Table 1.

Supporting information

Crystallographic data (excluding structure factors) for the structure reported in this article have been deposited with the Cambridge Crystallographic Data Centre as supplementary publication number CCDC 731786. Copies of the data can be obtained free of charge on application to CCDC 12 Union Road, Cambridge CB21 EZ, UK (Fax: (+44) 1223 336-033; e-mail: data_request@ccdc.cam.ac.uk).

Computational procedures and methodology

The geometry optimizations of canonical OH and NH form of the compound leading to energy minima in vacuo were performed by using DFT calculations with the use of Becke's three-parameters hybrid exchange–correlation functional (B3LYP) [18] incorporating B88 gradient-corrected exchange [19] and Lee–Yang–Parr non-local correlation functional [20] by means of 6-311 + G(d,p) basis set implemented in Gaussian 03W program package [21]. Geometry optimization of the title compound was achieved by the application of Berny optimization algorithm [22]. The values of the convergence criteria in the optimization procedures for both tautomers are below 4.5×10^{-4} hartree/bohr for maximum force, 3.0×10^{-4} hartree/bohr for RMS force, 1.8×10^{-3} Å for maximum displacement, 1.2×10^{-3} Å for RMS displacement. To describe the potential barrier height for regarding intramolecular proton transfer in gas phase, a relaxed potential

Table 1 Crystal data and details of the structure refinement for the compound

Crystal data	
Chemical formula	$C_{13}H_{10}BrNO_3$
Color/Shape	Stick/Brown
Formula weight	308.13
Cell setting	Triclinic
Space group	*P-1*
Unit cell parameters	a = 6.998 (1) Å
	b = 7.469 (1) Å
	c = 12.337 (2) Å
	α = 103.40 (1)°
	β = 97.723 (6)°
	γ = 105.06 (1)°
Volume	589.1(2) Å^3
Formula Z	2
Density (calculated)	1.734 Mg m^{-3}
Abs. coeff. (μ)	3.488 mm^{-1}
Data collection	
Diffractometer/meas. meth.	STOE IPDS 2/ω-scan
T_{min}, T_{max}	0.289, 0.824
F(000)	308
h_{min}, h_{max}	−8, 8
k_{min}, k_{max}	−9, 9
l_{min}, l_{max}	−15, 15
R_{int}	0.12
Refinement	
Refinement method	Full matrix least-squares on F^2
Measured reflections	8034
Independent reflections	1614
Observed reflections	1103
Number of parameters	175
Goodness of fit on F^2	1.115
R indices [$I > 2\sigma(I)$]	$R_1 = 0.062$, $wR_2 = 0.106$
Weighting scheme	w = 1/ $[\sigma(F_0^2) + (0.0271P)^2 + 0.3641P]$ where $P = (F_o^2 + 2F_c^2)/3$
$(\Delta/\sigma)_{max}$	<0.0001
$\Delta\rho_{max}$, $\Delta\rho_{min}$ (eÅ^{-3})	0.31, −0.34

energy surface (PES) scan was performed on the optimized geometry of OH tautomeric form at the B3LYP/6-311 + G(d,p) level by changing the redundant internal coordinate [23] (O1–H1 distance) from 0.90 to 1.80 Å in every 0.05 Å. All of the remaining internal coordinates were fully optimized at each point in the scan process. Thus, it is possible to monitor the changes in covalent topology and molecular geometry of the compound throughout intramolecular proton transfer with the aid of this non-adiabatic approach.

Aromaticity of many diverse π-electron systems has become a quantitatively identified notion with the aid of Harmonic Oscillator Model of Aromaticity (HOMA) index [24–26]. HOMA index describes the average squared deviation of bond lengths from an average value as follows:

$$\mathrm{HOMA} = 1 - \left[\frac{1}{n}\sum_{j=1}^{n}\alpha_j(R_j - R_{opt})^2\right],$$

where n is the number of bonds taken into the summation, R_j stands for a running individual bond length, α_j regarded as a normalization constant is equal to 257.7 for C–C, 93.52 for C–N, and 157.38 for C–O bonds, fixed to give HOMA = 0 for nonaromatic Kekulé systems and HOMA = 1 for purely aromatic systems with all bonds equal to the optimal value R_{opt} = 1.388 Å for C–C, R_{opt} = 1.334 Å for C–N, R_{opt} = 1.265 Å for C–O [24].

Results and discussion

As suggested by the results from spectroscopic means, molecular geometry of the compound shown in Fig. 1 [27] is in NH tautomeric form. Details of molecular geometry provide further information regarding the covalent topology and resonance effects. Some selected geometric parameters experimentally obtained and theoretically calculated are listed in Table 2. C1–Br1 bond length [1.895(7) Å] is comparable with that [1.899 Å] reported in [28]. The molecular geometry of the compound is almost planar with dihedral angle between the rings of 8.26(7)°.

It is well known that the heteroatom bonds are those most affected by molecular self-isomerization (intramolecular proton transfer). In this regard, C13–O1 and C7–N1 bonds are the most sensitive indicators of the structural form of the compound. The former is of single bond character in OH (phenol-imine) tautomers and of double bond character in canonical NH (keto-amine or quinoid) tautomers, while the latter is of double bond in OH (phenol-imine or benzenoid) tautomers and of single bond in canonical NH (keto-amine) tautomers as shown in Chart 1b. While C13–O1 bond length (Table 2) is in well agreement with those of similar NH (*cis*-keto amine) tautomers in the literature [29–33], C7–N1 and C7–C8 bond lengths are somewhat longer than their corresponding values in [29–33], indicating more single bond character of them. Although C_{ar}=C(sp^2) bond distances in these compounds varies from 1.391 to 1.404 Å [29–33], it is found as 1.412(9) Å in this study. As a result of partial quinoid effect in the compound, C7–C8 bond length is essentially intermediate between single and double C_{ar} to C(sp^2) bonds those in NH [29–33] and OH [34] tautomers. Depending on proton transfer, not only do the most indicative bonds vary, but also certain C_{ar}–C_{ar} bond lengths (Chart 1b) deviate from their optimal values (1.388 Å) and thus, aromaticity

of the ring involving proton transfer is decreased [1]. HOMA index is a useful tool to describe collectively degree of such bond-length deformations of the ring involving proton transfer. HOMA index of the ring through C8 to C13 atoms is found as 0.663. Comparing this value with the HOMA index of aromatic benzene (1.00), it can be stated that π-electron delocalization of the aromatic ring involving proton transfer is considerably deformed. This value is convenient with the fact that SAs in NH form are less stable due to their loss of ring aromaticities. Although SA derivative reported here is in NH form, its geometric parameters are deviate from their relevant values. These differentiations in certain bond distances can be explained by the resonance effect between two canonical structures, the *cis*-keto tautomer and zwitterionic form [5, 12, 13]. Throughout solid-state tautomerization, the proton initially attached to O1 is transferred to N1 by forming N–H···O type resonance-assisted H-bond (RAHB) whose details are given in Table 3, thereby introducing with appreciable keto character to the C13–O1 bond and partial double bond character to the C7–C8 due to the resonance effect mentioned before.

Three primary intermolecular interactions are observed in the crystal structure. O2–H2···O1 type H-bond gives rise to the formation $R_2^2(10)$ centrosymmetric pseudo-cyclic synthons stacking along *b*-axis as shown in Fig. 2. Ten-membered pseudocycles are adapted to chair conformation on O2–H2···O1 having symmetry center at (1/2, 1, 0). The existence of *ortho* and *meta* substituent groups in aromatic ring involving proton transfer creates a structural pattern that allows for the two-points self-recognition through supramolecular synthons. Due to O2–H2···O1 H-bond, H2 atom deviates from the plane through aromatic ring involving proton transfer by 0.32(7) Å. In addition, separations from Cg1 at (x, y, z) to Cg2 at ($-x$, $1-y$, $-z$) and Cg2 at (x, y, z) to Cg1 at ($-x$, $1-y$, $-z$) are found as 3.592(4) Å and 3.593(4) Å, where Cg1 and Cg2 stand for the centroids of the respective mean planes through C1 to C6 and C8 to C13 atoms. It can be shown that $\pi\cdots\pi$ interactions allowed by almost planar geometry of the compound serve to be strengthened the stacking of $R_2^2(10)$ synthons in the direction of *b*-axis.

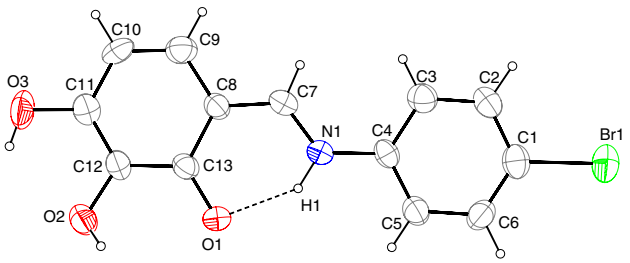

Fig. 1 Thermal ellipsoid view of the compound with the atomic numbering scheme. Intramolecular H-bond is illustrated by *dashed line*. Displacement ellipsoids are drawn at the 50% probability level and H atoms are shown as small spheres of arbitrary radii

Examining tautomerism process of the compound and its effects on the molecular geometry, it is possible to obtain valuable structural information regarding the compound. Stabilization levels of the limiting tautomers (phenol-imine and canonical *cis*-keto-amine) are very close to each other. Dependency of the relative energy of the compound, which are calculated regarding the absolute minimum for which $E = -3353.614$ a.u., against scan coordinate d(O–H) is shown in Fig. 3. Optimized OH tautomer of the compound is expectedly more stable than optimized NH form by 0.5 kcal/mol. In spite of this very small energy difference, potential barrier between two limiting tautomers of the compound is approximately found as 3.6 kcal/mol and this value is comparable with those (4.8 and 3.4 kcal/mol) reported in [35]. It is inferred from Fig. 3 that PES associated with the intramolecular proton transfer has two minima: While the global minimum corresponds to its stable OH form, the local one represents stable NH form. The activation energy of the transition from the global minimum to the local minimum is sufficiently small and this excitation is accompanied by intramolecular proton transfer from the hydroxyl group to the N atom. The large curvature of the potential energy for proton transfer in vicinity of the phenol-imine wall (Fig. 3) is associated with a large zero-point energy contribution in the ground state vibrational mode, which destabilizes the phenol-imine form [35]. Furthermore, a stable NH tautomer is observed for the compound.

Because of electronic redistribution during proton transfer, the two rings rotate around the C7–C8 and N1–C4 axis, ultimately resulting in planar molecular geometry as shown in Fig. 4. Optimized OH geometry of the compound is initially adapted nonplanar geometry with dihedral angle between the rings of 37.20°. Progressing proton transfer process, molecular geometry becomes planar gradually, in particular beyond 1.45 Å of the scan coordinate. The accomplished planarization of the compound has destabilized the parent phenol-imine tautomer by 0.5 kcal/mol. This can be explained by the increased basicity of N atom in planar conformation [36] preventing the lone-pair electrons on N to be conjugated with the phenol ring and the steric hindrance between H atoms bonded to C3 and C7. The distance between these H atoms is gradually decreased from 2.297 to 2.095 Å throughout the scan process.

Apart from these, certain characteristic changes are observed in covalent topology of the compound as shown in Fig. 5. These changes supply important information tautomerism in SA derivatives. It is inferred from the results in Fig. 5 that indicative bond lengths cannot reach their expected values even if tautomerization occurs in gas phase. At the seventeenth scan step equivalent to the stable

Table 2 Some selected geometrical parameters of the compounds (Å,°) obtained from X-ray crystallographic and computational study

	X-ray	DFT/B3LYP		X-ray	DFT/B3LYP
Bond lengths					
C8–C9	1.425 (9)	1.436	C7–C8	1.412 (9)	1.394
C9–C10	1.350 (9)	1.368	C7–N1	1.316 (8)	1.336
C10–C11	1.41 (1)	1.429	C13–O1	1.290 (8)	1.279
C11–C12	1.368 (9)	1.378	C4–N1	1.412 (8)	1.404
C12–C13	1.425 (9)	1.427	C12–O2	1.371 (8)	1.369
C8–C13	1.441 (9)	1.458	C11–O3	1.362 (8)	1.359
Bond angles					
N1–C7–C8	123.2 (7)	122.65	C7–N1–C4	127.4 (6)	128.34
O1–C13–C8	121.7 (6)	123.94	C9–C8–C13	120.4 (6)	119.58
C11–C12–O2	117.5 (6)	119.70	O3–C11–C10	118.1 (7)	117.97
Torsion angles					
C7–C8–C13–O1	1.0 (8)	0.00	C8–C7–N1–C4	−180.0 (5)	−179.99
C3–C4–N1–C7	7.7 (8)	−0.05	C9–C8–C7–N1	−178.9 (5)	179.99
C5–C4–N1–C7	−173.2 (5)	179.97	C13–C8–C7–N1	0.3 (9)	−0.01

Table 3 Geometric details of H-bonds (Å, °) of the compound

D–H···A	D–H	H···A	D···A	∠D–H···A
N1–H1···O1	0.90 (2)	1.84 (6)	2.600 (6)	142 (8)
O2–H2···O1^{i}	0.79 (8)	1.95 (8)	2.667 (7)	152 (7)

Note: *D* donor, *A* acceptor. Symmetry operation used to generate equivalent atomic positions: (i) $1 - x$, $2 - y$, $-z$

NH tautomer, two of indicative bond lengths, C13=O1 [1.278 Å] and C7=C8 [1.394 Å], are far from their respective values of 1.222 and 1.333 Å in benzoquinones [28], whereas C7–N1 bond length [1.338 Å] at the last scan step is close to its convenient value of 1.339 Å [28]. It is worth noting that the changes in three of C–C bond lengths aromatic ring involving proton transfer, C8–C9, C8–C13, and C12–C13 (Table 2). While C13–O1 and C7=N1 bonds become double and single bond during the tautomerization, respectively, single bond character of C8–C13 is more pronounced than that of C12–C13 and C8–C9 due to constructive resonance effects from the changes triggered in C13–O1 and C7=N1 bonds, proceeding in two different routes on the molecular skeleton.

Dependency of HOMA index of phenol ring involving proton transfer is shown in Fig. 6a. The interrelation between HOMA values of phenol ring and scan coordinate *d*(O–H) is inversely quadratic, since HOMA is a quadratic function of deviations of C_{ar}–C_{ar} bond lengths from their optimum value. There are two different regimes observed for variation in aromaticity of phenol and chelate ring (Fig. 6a). As far as behaviors of aromaticity of the phenol and chelate ring under the value of 1.35 Å of the scan coordinate are concerned that the loss in aromaticity of the former is compensated by augmentation in aromaticity of the latter. For more distant values of the scan coordinate of 1.40 Å, aromaticity of both fragments is reduced with different extents. While pseudo-aromaticity of the chelate ring is slightly reduced, that of phenol ring maintains to decrease considerably. The presence of two different regimes in aromaticities of phenol and chelate ring can be monitored by variation in aromaticity of 4-bromophenyl ring as shown in Fig. 6b. Concomitant decrease in aromaticities of phenol and chelate ring beyond 1.40 Å of the scan coordinate causes to a further aromatization of 4-bromophenyl ring in a different regime (Fig. 6b). The loss of aromaticity in phenol ring is transferred into chelate

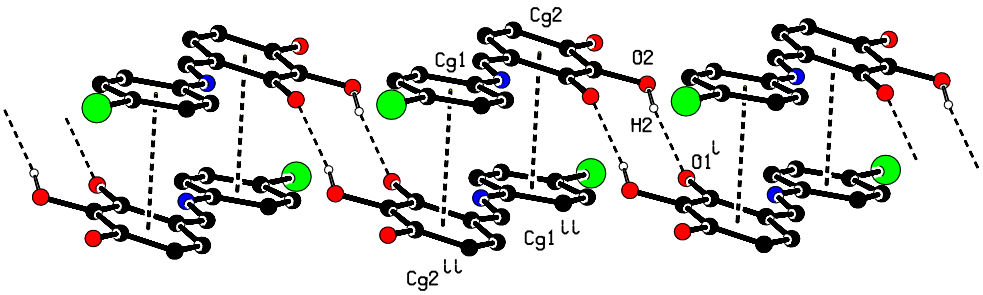

Fig. 2 Part of the stacking of $R_2^2(10)$ synthons along *b*-axis. H atoms not involved in the motif have been omitted for the sake of clarity

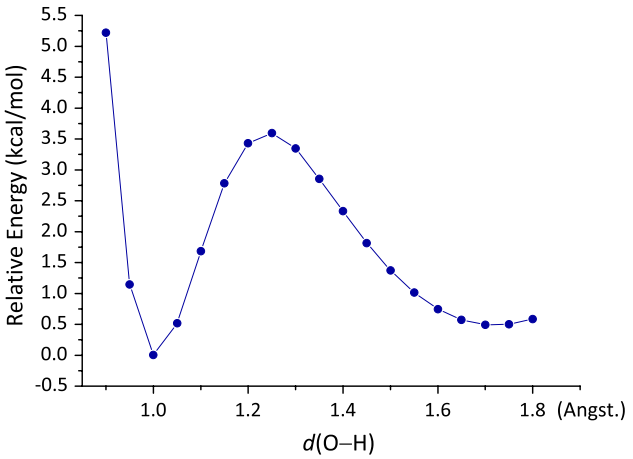

Fig. 3 Non-adiabatic potential curve for proton transfer of the compound in gas phase

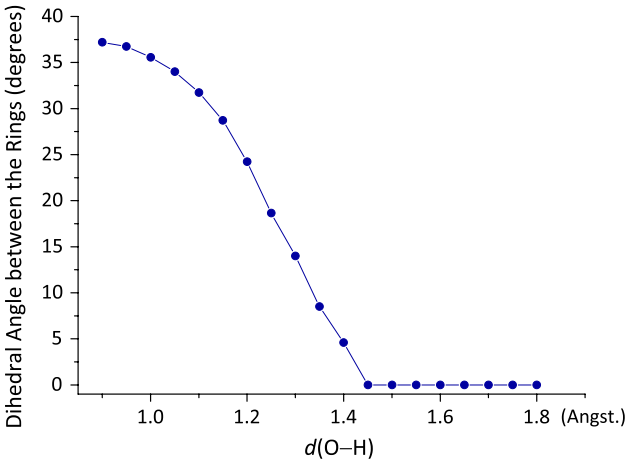

Fig. 4 Variation of the dihedral angle between the rings against the scan coordinate *d* (O–H)

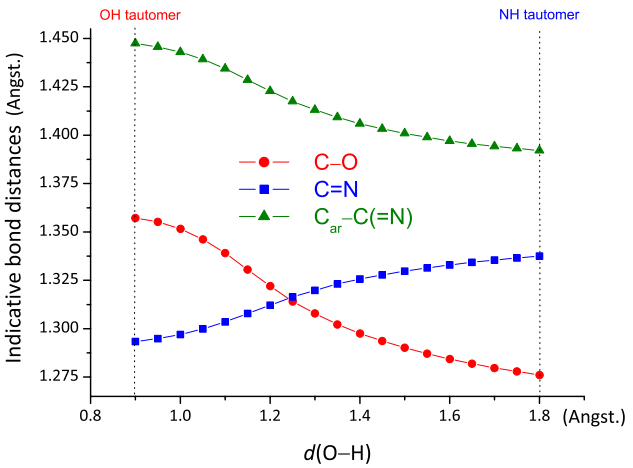

Fig. 5 Dependencies of the indicative bond lengths against the scan coordinate *d*(O–H)

ring to a large extent and into 4-bromophenyl ring to a little extent, indicating the presence of long-ranged π-electron coupling for the title compound. It is worth noting that aromaticity of the chelate ring in the NH form is approximately stable beyond the tautomeric transition state (O···H···N) due to the electronic redistribution of the rate of NH tautomeric forms, zwitterionic and *cis*-keto [37].

Pseudo-aromaticity of the chelate ring in the optimized OH tautomer of the compound (0.348) is less than that of the stable NH tautomer (0.672) as shown in Fig. 6a and is at a comparable level with that (0.380) reported in [38] for *o*-hydroxyaryl Schiff bases in OH tautomeric form containing only one aromatic fragment. It is inferred from these results that increase in the aromaticity of chelate ring supplies primary contribution to stabilization of NH tautomer. The reason for that HOMA index (0.380) of the chelate ring in *o*-hydroxyaryl Schiff bases for incipient

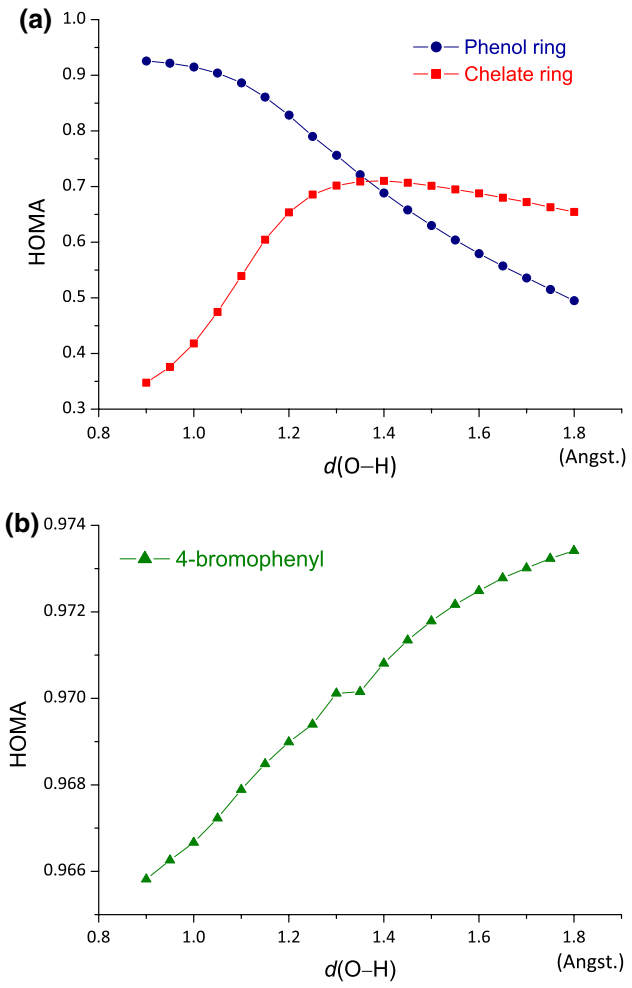

Fig. 6 Dependence of HOMA values of the ring involving proton transfer (**a**), chelate ring (**a**) and 4-bromophenyl ring (**b**) against the scan coordinate *d*(O–H)

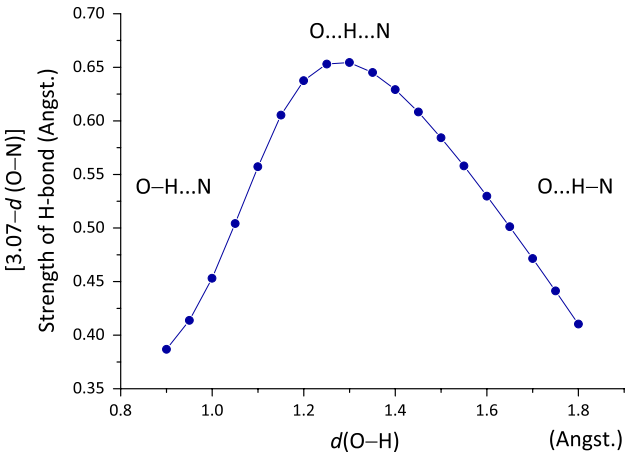

Fig. 7 Dependence of the strength of intramolecular H-bond against the scan coordinate *d*(O–H)

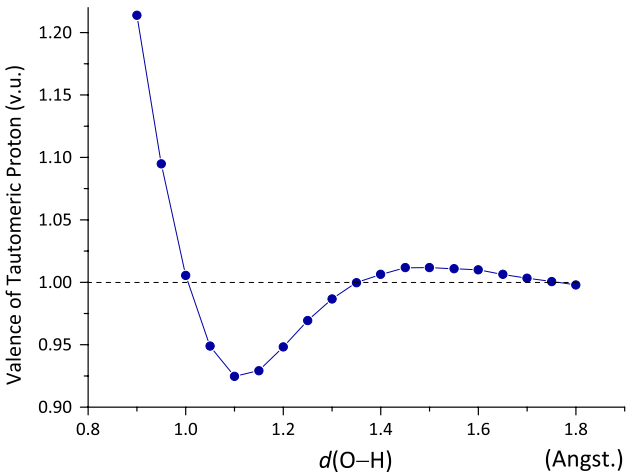

Fig. 8 Variation in the valence of tautomeric proton against the scan coordinate *d*(O–H). *Dashed line* shows formal valence level ($s = 1$) of tautomeric proton

H-bond [38] is more than that (0.348) in the title compound can be explained by the absence of another aromatic ring to which a portion of phenol ring aromaticity is transferred, giving rise to the lack of π-electron coupling. Pseudo-aromaticity of the chelate ring in the X-ray geometry of the compound is 0.749, slightly more than its corresponding value (0.703) in [37]. The difference between the levels of pseudo-aromaticity of chelate ring reported here and that in [37] is essentially related to covalent skeleton of π-donor fragments, phenol, and naphthalen-2-ol. Aromaticity for one of the fused six membered rings in naphthalen-2-ol, which does not contain *o*-hydroxyl, is increased while that of the other one is decreased [37]. For this reason, π-electron coupling between naphthalen-2-ol and the chelate ring is deficient as compared with that of the title compound. On the other hand, difference between these pseudo-aromaticities may be attributed to the strength of the associated intramolecular H-bonds playing a central role in tautomerism of SA derivatives. The strength of intramolecular H-bond is quantitatively described as a difference between the sum of the non-covalent van der Waals radii [39] of N and O atom (3.07 Å) and the distance from N to O atom. Variation of the strength of intramolecular H-bond throughout the scan process is shown in Fig. 7. According to Fig. 7, the most strength intramolecular H-bond of the compound is observed for tautomeric transition states (O··· H···N) rather than those in either O–H···N or O···H–N tautomeric forms. This inference is in agreement with those reported by Filarowski and his colleagues for distinct Schiff base species in [3, 37, 40].

An elegant way to investigate heteronuclear H-bonds is based on the valence (or bond order) calculations [11], providing a quantitative evaluation for the valence of tautomeric proton. Valence of H atoms in N···H–O and O···H–N bond is calculated as $s = \exp[(r_0 - r)/b]$ in valence units (v.u.), where $b = 0.371$ for O–H and $b = 0.385$ for N–H, r stands for the distance between H and acceptor or donor atom, r_0 is equal to 0.942 for O–H and to 0.992 for N–H [11]. The rule of bond order conservation requires that summation of the calculated s values for tautomeric proton ($s_{\mathrm{O–H}} + s_{\mathrm{H\cdots N}} = s_{\mathrm{O\cdots H}} + s_{\mathrm{H–N}}$) is formally equal to 1.00. Variation of total bond valence of tautomeric proton with scan coordinate is shown in Fig. 8. According to Fig. 8, valence of tautomeric proton has monotonically decreased by incipient proton transfer until it reaches to a minimum value (0.925) from relatively high initial valence value of 1.214. It augments increasingly with the growing predominance of the NH form (canonical *cis*-keto or zwitterionic) to compensate deficiency in electronic population on tautomeric proton and then, converges slightly over its formal value of 1.00 toward stable NH tautomer. Considering valence of tautomeric proton of both the stable OH tautomer appeared in third step and stable NH tautomer appeared in the vicinity of seventeenth step, it can be stated that stable tautomers are observed in the vicinity of formal valence of tautomeric proton. Molecular structures corresponding to below this value are regarded as tautomeric transition states, whereas tautomeric protons in stable OH and NH tautomers in crystal phase have a considerably higher value of 1.00. This inference is confirmed by H-bonds reported in [37, 40]. Valences of tautomeric proton located in the center of the hydrogen bridge are obtained as 0.829 and 0.905 with regard to geometric details of H-bonds in [37, 40], while those of other stable tautomeric forms in [37, 40] are higher than 1.00 in the interval of 1.015–1.214. Total valence of the tautomeric proton in the crystallographically observed geometry of the compound is found as 1.376 and this value is in the interval of 1.070–1.487 calculated for the similar compounds [29–33]. It is inferred from these computational results that

excess valence of the tautomeric proton in the initial OH form leads to proton transfer reaction and the tautomerization results in almost formal single valence of the tautomeric proton for both stable OH and NH form in gas phase. Relatively high values of the valence of tautomeric proton in stable tautomeric forms mentioned above can be explained by the fact that hydrogen bonds rarely adopt their optimal geometry in solid state, since crystal-packing forces can easily bend, elongate and compress them.

Valence of tautomeric proton in transition states is reduced to below its formal value of 1.00, indicating partial positive charge ($+\delta$) on tautomeric proton. Although intramolecular H-bond has an electrostatic origin, this character may be obscured by charge flow through π-bonds in SAs. However, a subtle fact regarding mutual dependence in aromatization levels, i.e., concomitant decrease in aromaticitiy of phenol and chelate ring beyond 1.40 Å of the scan coordinate remains unclear. This behavior can be understood by π-electron transfer from phenol ring to the chelate ring and furthermore from the chelate ring to low-lying formally vacant p-type orbitals of $H^{+\delta}$ cation and π-conjugated system of 4-bromophenyl ring as illustrated in Chart 2, since hydroxyl group becomes a stronger π-donor by incipient proton transfer [38]. Slight decrease in valence of tautomeric proton beyond 1.45 Å of the scan coordinate (Fig. 8) indicates weak π-back donation toward chelate ring at ignorable level, so that its valence is eventually reduced to 1.00. These considerations regarding the compound are convenient with the fact that intramolecular RAHB is formed by π-bond cooperativity [41]. Soon after the saturation in aromaticity of chelate ring or equivalently planarization of the molecular geometry (Fig. 4), electronic redistribution of the molecule results in the increase of N–C_{ar} bond length as shown in Fig. 9, which becomes harder π-electron transfer to 4-bromophenyl ring. Thus, the chelate ring also contributes to π-electron donation toward 4-bromophenyl ring at least in part, leading to slight decrease in its aromaticity as shown in Fig. 6a.

These particular observations suggest that the proton transfer process is balanced by the changes in π-conjugated system of the phenol, chelate, and distant aromatic 4-bromophenyl ring. Furthermore, it can be stated that dynamic balance between phenol ring and adjacent chelate ring facilitates obtaining the NH form as previously reported in [1, 3, 37]. Stabilization of the pseudo-aromatic ring is increased with increasing its HOMA index. Thus, pseudo-aromatic chelate ring formation is established to compel a reduced aromaticity in phenol ring. Intramolecular RAHB mediates the mentioned dynamics observed in the aromatization levels. In addition, some structural remarks may be concluded considering variations in HOMA values. It is known that aromaticity is affected by non-covalent interactions such as H-bonds and $\pi \cdots \pi$.

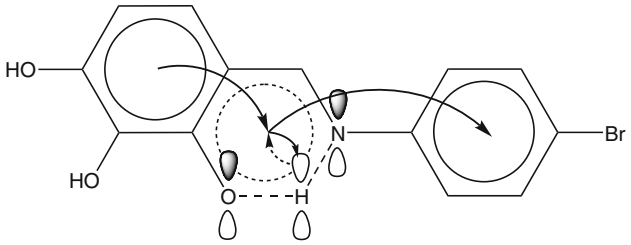

Chart 2 Schematic representation charge flow through π-bonds accompanying tautomerization process in the compound. *Dashed arrow* denotes π-back donation

Although aromaticity of the phenol ring is considerably deformed during the tautomerization, its π-electron delocalization level in the crystal structure is large enough to involve $\pi \cdots \pi$ interactions. In other words, while hydroxyl bond elongation causes to dearomatization of the phenol ring, molecular stacking pattern in the crystal structure enforces to hold aromaticity of phenol ring at a relatively high level (HOMA = 0.663). At this point, it should be pointed out that depending on the proton transfer HOMA index of aromatic rings carrying O atom in *ortho* position may be reduced to 0.310 for *o*-hydroxyaryl [1] and to 0.5–0.2 for naphthaldimine Schiff-bases [37].

Small energetic difference between canonical OH and NH tautomers may be understood discrepancies between the associated molecular geometries. Conformational discrepancies among the crystallographically observed geometry, the energy minimized NH and OH form of the molecule were quantitatively analyzed by r.m.s. overlays including H atoms as shown in Fig. 10. A least-squares fit of the optimized OH with the optimized NH form gives an r.m.s. deviation of 0.091 Å, while that of the optimized NH form with the crystallographically observed geometry of the compound gives an r.m.s. deviation of 0.014 Å. The conformations of NH and OH form of the compound are considerably different due to the position of tautomeric proton and the rotation about the N1–C4 bond. In addition, intramolecular H-bond is fundamental in determining the crystallographically observed geometry of the compound, since the slightly large value of the angle N1–C7–C8 (Table 2) may be due to intramolecular H-bond and reduces chelate ring strain.

Conclusion

Spectroscopic and crystallographic results show that the compound is in NH tautomeric form. Indicative bond lengths in the compound deviate from their expected values in the crystal phase at a certain extent due to a possible through-resonance effect between canonic NH (*cis*-keto) and zwitterionic form of the compound. Changes in

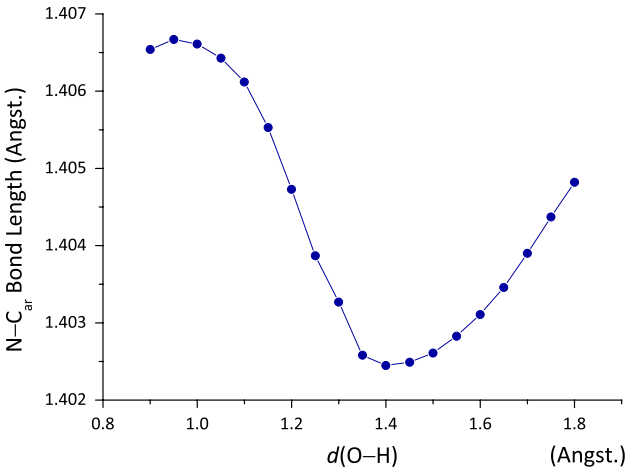

Fig. 9 Dependency of N–C_{ar} bond length against the scan coordinate *d*(O–H)

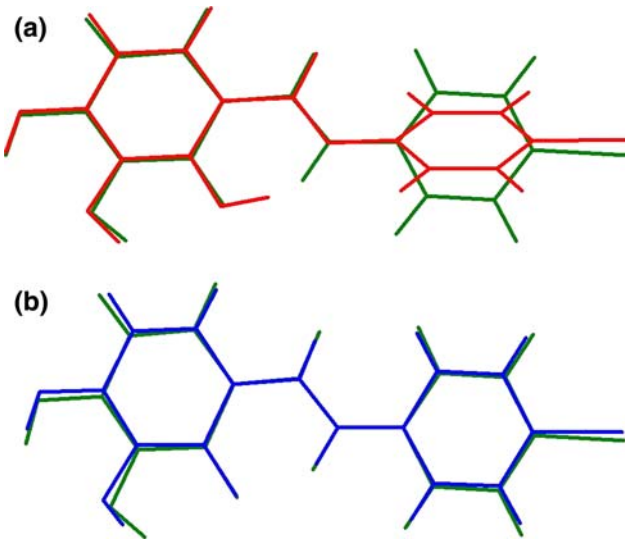

Fig. 10 Superimpositions of the optimized OH (*red*) and NH (*green*) form (**a**) and the crystallographic conformation (*blue*) and the optimized NH form (**b**). (Color figure online)

both covalent topology and molecular geometry of the compound accompanying proton transfer were monitored by a relaxed PES scan with respect to hydroxyl bond length. At this point, Ogawa and Harada conjecture [5] regarding SAs in NH form should be corrected so as to cover the results here. The most important result from our study is that indicative bond lengths cannot reach their expected values even if proton transfer occurs in gas phase, whereas Ogawa and Harada [5] claimed that SAs in NH form are predominantly *cis*-keto in the gas phase. Although zwitterionic and *cis*-keto form of SAs seem to be identical in terms of atomic position, their covalent skeletons are very different from each other. In solid state, NH forms of SA derivatives are, in general, regarded as a superposition of these forms, but many authors have overlooked this fact and have been contented with qualifying them only keto-amine tautomer. Another revision for Ogawa and Harada conjecture [5] is associated with stabilization scenarios regarding SAs. According to Ogawa and Harada [5], stabilization of NH forms depends on structural changes by intermolecular interactions in an aggregation. Intermolecular contacts are, of course, significant for the stabilization of molecules in an aggregation such as crystal structure, but they are not sufficient to explain the reasons at molecular scale. On the other hand, Filarowski and his colleagues [1, 3, 37, 40] have emphasized that aromaticity balance is of importance in understanding of chemical background underlying tautomerism. Here we were intent to extend Filarowski's the concept of aromaticity balance to SA derivatives and to deepen the considerations for tautomerism in SA derivatives.

Quantum chemical study of the compound suggests that pseudo-aromatic chelate ring formation is established to compel a reduced aromaticity (or π-electron delocalization) in phenol ring, reflecting a dynamic balance between aromaticities of these adjacent fragments. In addition, a further aromatization of 4-bromophenyl ring during proton transfer reaction suggests the presence of long-ranged π-electron coupling in the compound. The proton transfer process occurring beyond 1.4 Å of the scan coordinate (Fig. 6a) causes to concomitant dearomatization of the phenol and chelate ring at different extents. This behavior can be explained by π-electron donation from the chelate ring to 4-bromophenyl ring in addition to donation from phenol ring due to the increase in N–C_{ar} bond length, becoming harder π-electron transfer to 4-bromophenyl ring. In this regard, it is reasonable to think that augmentation in aromaticity of the chelate ring has primary effect on the stabilization of NH tautomer and RAHB leading to chelate ring formation plays a central role in electronic redistribution due to electron delocalization path involving low-lying vacant p-type orbitals on the tautomeric proton. It is worth noting that intramolecular H-bonds in tautomeric transition states where proton is located at the center of H-bridge are stronger than those of stable tautomeric forms and RAHB affects the electronic state of its neighboring aromatic fragments.

Acknowledgments The authors wish to acknowledge Ondokuz Mayıs University for the use of the STOE IPDS 2 diffractometer purchased under grants F.279 and F.377.

References

1. Filarowski A, Kochel A, Cieslik K, Koll A (2005) J Phys Org Chem 18:986–993
2. Fabian WMF, Antonov L, Nedeltcheva D, Kamounah FS, Taylor PJ (2004) J Phys Chem A 108:7603–7612

3. Filarowski A (2005) J Phys Org Chem 18:686–698
4. Amimoto K, Kawato T (2005) J Photochem Photobiol C Photochem Rev 6:207–226
5. Ogawa K, Harada J (2003) J Mol Struct 647:211–216
6. Yildiz M, Kiliç Z, Hokelek T (1998) J Mol Struct 441:1–10
7. Nazir H, Yildiz M, Yilmaz H, Tahir MN, Ulku D (2000) J Mol Struct 524:241–250
8. Karabiyik H, Guzel B, Aygun M, Boga G, Buyukgungor O (2007) Acta Crystallogr C 63:o215–o218
9. Dominiak PM, Grech E, Barr G, Teat S, Mallinson P, Wozniak K (2003) Chem Eur J 9:963–970
10. Krygowski TM, Wozniak K, Anulewicz R, Pawlak D, Kolodziejski W, Grech E, Szady A (1997) J Phys Chem A 101:9399–9404
11. Steiner T (1998) J Phys Chem A 102:7041–7052
12. Petek H, Albayrak C, Agar E, Kalkan H (2006) Acta Crystallogr E 62:o3685–o3687
13. Karabiyik H, Ocak-Iskeleli N, Petek H, Albayrak C, Agar E (2008) J Mol Struct 873:130–136
14. Ogawa K, Harada J, Tamura I, Noda Y (2000) Chem Lett 29:528–529
15. Stoe and Cie (2002) X-AREA (Version 1.18) and X-RED32 (Version 1.04), Darmstadt, Germany
16. Farrugia LJ (1999) J Appl Cryst 32:837–838
17. Sheldrick GM (2008) Acta Cryst A 64:112–122
18. Hertwig RH, Koch W (1997) Chem Phys Lett 268:345–351
19. Becke AD (1988) Phys Rev A 38:3098–3100
20. Lee C, Yang W, Parr RG (1988) Phys Rev B 37:785–789
21. Frisch MJ, Trucks GW, Schlegel HB, Scuseria GE, Robb MA, Cheeseman JR, Montgomery JA, Vreven Jr, T, Kudin KN, Burant JC, Millam JM, Iyengar SS, Tomasi J, Barone V, Mennucci B, Cossi M, Scalmani G, Rega N, Petersson GA, Nakatsuji H, Hada M, Ehara M, Toyota K, Fukuda R, Hasegawa J, Ishida M, Nakajima T, Honda Y, Kitao O, Nakai H, Klene M, Li X, Knox JE, Hratchian HP, Cross JB, Adamo C, Jaramillo J, Gomperts R, Stratmann RE, Yazyev O, Austin AJ, Cammi R, Pomelli C, Ochterski JW, Ayala PY, Morokuma K, Voth GA, Salvador P, Dannenberg JJ, Zakrzewski VG, Dapprich S, Daniels AD, Strain MC, Farkas O, Malick DK, Rabuck AD, Raghavachari K, Foresman JB, Ortiz JV, Cui Q, Baboul AG, Clifford S, Cioslowski J, Stefanov BB, Liu G, Liashenko A, Piskorz P, Komaromi I, Martin RL, Fox DJ, Keith T, Al-Laham MA, Peng CY, Nanayakkara A, Challacombe M, Gill PMW, Johnson B, Chen W, Wong MW, Gonzalez C, Pople JA (2003) Gaussian 03, Revision E.01, Gaussian, Inc., Pittsburgh, PA
22. Schlegel HB (1982) J Comput Chem 3:214–218
23. Peng C, Ayala PY, Schlegel HB, Frisch MJ (1996) J Comp Chem 17:49–56
24. Krygowski TM (1993) J Chem Inf Comput Sci 33:70–78
25. Krygowski TM, Cyranski M (1997) In: Hargittai I, Hargittai M (eds) Advances in molecular structure research. JAI Press, London, pp 227–268
26. Kruszewski J, Krygowski TM (1972) Tetrahedron Lett 13:3839–3842
27. Farrugia LJ (1997) J Appl Cryst 30:568
28. Allen FH, Watson DG, Brammer L, Orpen AG, Taylor R (2004) In: Prince E (ed) International tables for crystallography (vol. C): mathematical, physical and chemical tables, 3rd edn. Kluver Academic Publishers, Dordrecht, pp 790–811
29. Ersanli CC, Albayrak C, Odabasoglu M, Erdonmez A (2003) Acta Crystallogr C 59:o601–o602
30. Sahin O, Albayrak C, Odabasoglu M, Buyukgungor O (2005) Acta Crystallogr E 61:o2859–o2861
31. Sahin O, Buyukgungor O, Albayrak C, Odabasoglu M (2005) Acta Crystallogr E 61:o1579–o1581
32. Petek H, Albayrak C, Odabasoglu M, Senel I, Buyukgungor O (2008) J Chem Crystallogr 38:901–905
33. Kosar B, Buyukgungor O, Albayrak C, Odabasoglu M (2004) Acta Crystallogr C 60:o458–o460
34. Moustakali-Mavridis I, Hadjoudis E, Mavridis A (1980) Acta Crystallogr B 36:1126–1130
35. Popovic Z, Pavlovic G, Roje V, Doslic N, Matkovic-Calogovic D, Leban I (2004) Struct Chem 15:587–598
36. Marston CC, Balint-Kurti G (1989) J Chem Phys 91:3571–3576
37. Filarowski A, Kochel A, Kluba M, Kamounah FS (2008) J Phys Org Chem 21:939–944
38. Krygowski TM, Zachara JE, Moszynski R (2005) J Chem Inf Model 45:1837–1841
39. Bondi A (1964) J Phys Chem 68:441–451
40. Filarowski A, Koll A, Glowiak T (2002) J Chem Soc Perkin Trans 2:835–842
41. Steiner T (2002) Angew Chem Int Ed 41:48–76